Time-varying Atmospheric Waveguides - Climatologies and Connections to Quasi-Stationary Waves

Rachel H. White[1]

[1]Department of Earth, Ocean and Atmospheric Sciences, University of British Columbia, Vancouver, BC, Canada

Correspondence: Rachel H. White (rwhite@eoas.ubc.ca)

Abstract. Atmospheric waveguides have been linked to amplified atmospheric Rossby waves and therefore to extreme weather events in the mid-latitudes. Waveguides have often been calculated on zonal-mean data, and/or on timescales of a month or longer. Here, I develop an objective algorithm to detect barotropic waveguides, and create a dataset of time- and spatially-varying waveguides in both summer and winter for both the Northern and Southern Hemisphere (NH/SH), including a metric of waveguide depth. In this dataset, waveguides for waves of zonal wavenumber 5 exist in the extra-tropics on more than 40% of days across many longitudes, with the frequency of occurrence reducing for higher zonal wavenumbers. Waveguides tend to be more frequent, and deeper, in summer than in winter, and more frequent in the NH than the SH. Composites of days with high spatial mean waveguide depth over particular regions show a double jet structure associated with strong waveguide occurrence, consistent with previous research. Significant positive correlations exist between waveguide depth and the presence/strength of quasi-stationary waves. In the SH these correlations are strong across much of the mid-latitudes in both seasons, whilst in the NH significant correlations are found only over the Atlantic, Europe and Asia during NH summer, with the strongest correlations over the Atlantic and western Europe, a region notable for its strong positive trend in extreme heat temperature events in recent decades.

1 Introduction

The circulation associated with large scale atmospheric Rossby waves (Rossby, 1939) is known to be associated with extreme weather (e.g. Bosart et al., 1996; Screen and Simmonds, 2014; Chen et al., 2015; Hoskins and Woollings, 2015; Wirth et al., 2018; White et al., 2022). This includes temperature extremes (e.g. Marengo et al., 2002; Teng et al., 2013; Parker et al., 2014; McKinnon et al., 2016; Wolf et al., 2018; Röthlisberger et al., 2019), as well as extreme precipitation and related flooding (e.g. Blackburn et al., 2008; Schubert et al., 2011; Hirata and Grimm, 2016; Vries and Jan, 2021). The connection to temperature extremes is thought to be particularly strong for waves that become quasi-stationary, i.e. have near-zero phase speed, and thus exhibit circulation anomalies that are persistent in space for many days (Wolf et al., 2018; Röthlisberger et al., 2019; Ali et al., 2021), and/or high amplitude (Petoukhov et al., 2016; Jiménez-Esteve et al., 2022). The mechanisms underlying this quasi-stationary and amplifying behaviour are not yet fully understood (e.g. Screen and Simmonds, 2013a; White et al., 2022), and there is particular uncertainty around how such mechanisms might be impacted by anthropogenic climate change and related Arctic amplification (Francis and Vavrus, 2012; Coumou et al., 2018; Blackport and Screen, 2020). It has been

suggested, however, that the jet configurations that create 'atmospheric Rossby waveguides' (e.g. Martius et al., 2010) may play an important role in the amplification of Rossby waves and any future changes in such waves (Hoskins and Woollings, 2015; Petoukhov et al., 2016; Mann et al., 2017; White et al., 2022); improved understanding of atmospheric waveguides and their role in the existence and amplification of quasi-stationary waves is therefore of great interest.

30   Atmospheric Rossby waveguides are regions of the atmosphere in which the background circulation, due to strong meridional gradients in potential vorticity (PV), provides a preferred, typically zonally oriented, pathway for the propagation of Rossby waves. Such gradients are associated with atmospheric jets (Manola et al., 2013; Wirth et al., 2018; Branstator and Teng, 2017; Hoskins and Karoly, 1981; Hoskins and Ambrizzi, 1993; Martius et al., 2010; Giannakaki and Martius, 2016), although in a full baroclinic atmosphere, meridional gradients in PV can also result from meridional gradients in static sta-
35 bility. Recent studies, however, have suggested that quasi-stationary waves are largely equivalent barotropic, and thus the barotropic approximation may be sufficiently applicable to provide useful insights into the behaviour of quasi-stationary waves (e.g. Petoukhov et al., 2013). Through the linearization of the barotropic equations, Hoskins and Karoly (1981) developed a simple theory for the propagation of waves in a barotropic atmosphere. This theory includes the definition of a 'stationary wavenumber' of the background flow, the wavenumber for which a Rossby wave would become stationary in that flow. The
40 spatial distribution of this stationary wavenumber field dictates how waves will propagate, allowing 'ray tracing' – calculation of the expected pathway of a theoretical Rossby wave for the given background flow. Despite the limitations of this theory (e.g. Wirth, 2020), including questionable validity of the underlying assumptions (limitations articulated clearly in the original papers), the theory provides qualitatively useful insights into the behaviour of waves in both idealized simulations and with realistic flow conditions (Hoskins and Karoly, 1981; Hoskins and Ambrizzi, 1993; Hsu and Lin, 1992; Hoskins and Woollings,
45 2015; White et al., 2017).

The theory of atmospheric waveguides has been used to understand the propagation of Rossby waves on a range of timescales, from climatological or seasonal means (Hoskins and Ambrizzi, 1993; Ding and Wang, 2005; Branstator, 2014) to waves associated with extreme events with durations of between one week to one month (Petoukhov et al., 2013). One of the key requirements of linear waveguide theory is that there is a clear separation between the 'waves' and the 'background flow' on
50 which the waves propagate. Without this clear separation between the background flow and the waves, much care must be taken in the interpretation of results (Andrews, 1985; Held et al., 2002), especially with the non-linear flows often associated with extreme events (White et al., 2022). A relatively common approach for the separation of waves and background flow is to take the longitudinal (zonal) mean as the background flow, and waves as deviations from this zonal mean (e.g. Hoskins and Karoly, 1981; Petoukhov et al., 2013, 2016). An extension to this is to use a 'zonalized' flow, in which PV is conserved during
55 the calculation of a zonal mean flow (e.g. Nakamura and Zhu, 2010; Nakamura and Solomon, 2011; Methven and Berrisford, 2015). Particularly in the Northern hemisphere, however, the tropospheric jets vary substantially with longitude, affecting the waveguides, and thus the propagation of waves (Branstator, 1983; Branstator and Teng, 2017). More recent work has extended this PV zonalization technique to a longitudinally-varying zonalized flow (Polster and Wirth, 2023). Another alternative approach is to take a time mean circulation as the background flow, in which climatological or seasonal means are considered
60 as the background flow (e.g. Hoskins and Ambrizzi, 1993). This works well for understanding climatological pathways of

waves; however, when using waveguides to understand extreme events, which by definition occur for a limited period, it may be helpful to understand how a time-varying background flow affects the probability of high-amplitude quasi-stationary waves developing. Further complicating this separation of waves and background flow, waves can themselves feedback onto and impact the 'background' zonal wind (Lorenz and Hartmann, 2003; Limpasuvan and Hartmann, 2000). Even without feedbacks,
65   (Wirth and Polster, 2021) show that a high amplitude non-linear wave can create zonal mean conditions consistent with a waveguide, and so a correlation between waveguides and waves does not imply that waveguides are causing the waves.

To better understand and study the connections between atmospheric waveguides and quasi-stationary waves, in this study an objective algorithm is developed, using the barotropic stationary wavenumber waveguide definition of Hoskins and Karoly (1981); Hoskins and Ambrizzi (1993) to identify waveguides on zonally- and time-varying flow. This algorithm is applied to
70   ERA5 re-analysis data (Hersbach et al., 2020) to produce maps of waveguide presence and strength from 1980 to 2022. This is, to the author's knowledge, the first such dataset of observed waveguides. This dataset is explored to examine the climatological statistics of barotropic waveguides, the zonal wind conditions typically associated with waveguides, and correlations with quasi-stationary waves.

2   Data and pre-processing

75   ERA5 re-analysis data (Hersbach et al., 2020) are used in this study as an approximation of the observed state of the atmosphere for calculation of waveguides and quasi-stationary waves. Zonal and meridional wind data are downloaded at 6-hourly temporal resolution, before being averaged into daily means. The data are regridded to a regular latitude-longitude 1×1 ° grid using the Climate Data Store API (Hersbach et al., 2023). Following Hoskins and Karoly (1981); Hoskins and Ambrizzi (1993); Petoukhov et al. (2013); Wolf et al. (2018), winds at $300hPa$ are used for both the waveguides and the waves, although this is
80   slightly higher than the equivalent barotropic level of $425hPa$ estimated by Held et al. (1985).

2.1   Background flow

As discussed in the introduction, filtering of the atmospheric circulation fields is required to separate the waves from the slowly-varying background flow that may act as a waveguide. This problem is non-trivial, and there is no single definition of the slowly-varying background flow. In this study I follow Branstator (1983), and calculate background flow conditions
85   by filtering the zonal wind using a fast Fourier Transform, and retaining only zonal wavenumbers $k = 0$, 1 and 2. Using these wavenumbers provides some spatial scale separation from the quasi-stationary waves, discussed in the following section, which retain only zonal wavenumbers 4-15. Sensitivity tests in which zonal wavenumber 3 is also retained when calculating the waveguides shows no sensitivity of the main conclusions to this choice (see Section 5.1). As noted by Wirth (2020), zonal mean filtering does not remove the effects of non-linear waves such as blocking events, and similar arguments can be made
90   for the Fourier filtering applied here. Caution is therefore still required in interpreting the results of this analysis, particularly when considering the direction of any causality between waveguides and waves.

A time filter is also applied to further remove impacts of transient waves from the background flow. A simple running mean filter of 15 days is used, chosen to be compatible with the time filtering commonly used for quasi-stationary waves (e.g. Wolf et al., 2018; Röthlisberger et al., 2019). As with the zonal filtering, this will not remove all traces of non-linear waves such as

95 blocking, even if they do occur on timescales shorter than that of the filter. In Section 5.1 I show that the conclusions of this paper are unaffected by using a 10 day filter instead of 15 days.

2.2 Quasi-stationary waves

One of the main interests in atmospheric waveguides is their potential connection to high-amplitude quasi-stationary waves (QSWs) that can lead to extreme weather. Here a method of extracting the envelope of QSWs is used, following Wolf et al.

100 (2018). This method calculates a running mean on meridional wind data to isolate quasi-stationary waves, applies a fast Fourier transform to select the planetary wavenumbers of interest, and then uses a Hilbert transform to calculate the amplitude of the wave envelope, following Zimin et al. (2003). Following the application of a 15-day running mean to daily mean meridional wind data, v, a smoothed daily climatology is calculated using a Savitzky-Golay filter of order 1, with a 51 day window. Anomalies from this climatology, v', are then used to calculate quasi-stationary waves using a Hilbert transform. Whilst pre-

105 vious studies have used a latitude-dependent wavelength filter (e.g. Wolf et al., 2018), here a fixed wavenumber range of 4-15 is used at all latitudes to maintain a similar separation from the background flow at each latitude. The sensitivity of this choice is tested, showing that it makes a noticeable difference, particularly at high latitudes, confirming that care is required to interpret the separation between waves and the background flow. Wolf and Wirth (2015) note that the semi-geostrophic nature of Rossby waves often results in the Hilbert transform separating a single Rossby wavepacket into fragments; for simplicity, a

110 semi-geostrophic transformation is not applied here — the QSW envelope field is averaged over 20° longitude, reducing the impacts of the fragmentation.

3 Waveguide identification

To identify the presence of a waveguide, we follow the definition of Hoskins and Karoly (1981) and Hoskins and Ambrizzi (1993) based on the linearized barotropic PV equation, with the assumption that meridional gradients in PV will dominate

115 in the background flow, as in Hoskins and Ambrizzi (1993). This approach first calculates a diagnostic called the *stationary wavenumber*, K_s and then defines a waveguide for wavenumber k as a region of finite $K_s > k$ bounded to both the north and south by 'turning points' (TPs) or 'turning latitudes' where $K_s = k$. The stationary wavenumber is calculated as:

$$K_s = a(\beta_M/U_M)^{1/2} \tag{1}$$

where a is the radius of the Earth, β_M is the meridional gradient of absolute vorticity, transformed onto a Mercator projec-

120 tion, and U_M is the Mercator basic zonal wind. Following Hoskins and Karoly (1981) and making use of the identities for differentiation on the Mercator projection given in Appendix A, these two variables are calculated as:

$$\beta_M = \frac{2\Omega cos^2\phi}{a} - \frac{cos\phi}{a^2}\frac{\partial}{\partial\phi}\frac{1}{cos\phi}\frac{\partial}{\partial\phi}(U_M cos^2\phi) \tag{2}$$

where

$$U_M = \frac{U}{cos\phi} \tag{3}$$

125   Once K_S has been calculated on the temporally and zonally filtered U, an algorithm identifies waveguides for waves of integer wavenumber k from 4 to 9. At each longitude, and time, the algorithm looks for regions where two turning points (TPs) exist, such that $k < K_s < \infty$ between the TPs and $K_s < k$ immediately outside of the TPs. This is illustrated in Fig. 1, in which K_s for a particular day and longitude is shown, with TPs identified for wavenumbers $k = 4, 5, 6$, and the hatching illustrating the waveguides for these different k. Once a waveguide is detected based on K_s, a minimum threshold is applied to the zonal

130   wind U within the waveguide, the maximum waveguide *depth*, $W_d = K_s - k$ within the waveguide, and to the waveguide *width*, W_w, the meridional distance between the TPs. These criteria limit detection to substantial waveguides within westerly flow. In the main results the following thresholds are used to define the presence of a waveguide: $U \geq 0.5 m/s$; $W_d \geq 1$; $W_w \geq 5°$ latitude. The two hemispheres are treated separately, and the algorithm only looks for TPs between 20-85° N/S. This therefore includes much of the sub-tropical jets, but reduces the influence of the cut-off latitude on waveguides in the extra-tropics. In

135   section 5.1 I show the the results within the mid-latitudes are largely insensitive to changing the equatorward cut-off to be 30° N/S. The minimum waveguide depth and width thresholds can be easily varied through input arguments to the algorithm, and in Section 5.1 I show that the main results of this paper are insensitive to the exact values chosen.
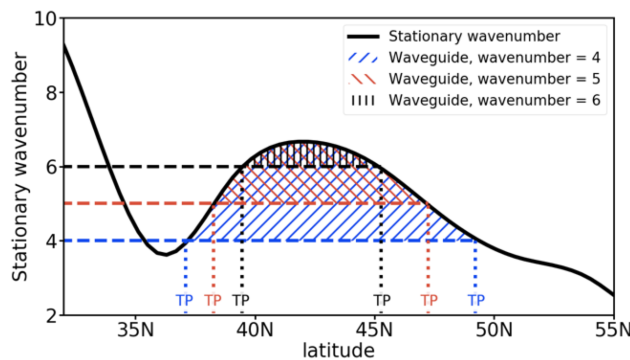
Figure 1. Illustration of the waveguide detection algorithm for a given day and longitude. The black thick line denotes the stationary wavenumber K_s as a function of latitude. The 'turning points' are marked as 'TP' for wavenumbers $k = 4$, 5 and 6. Shading illustrates where waveguides exist for these different wavenumbers.

     Once a waveguide has been detected, the algorithm saves the waveguide depth, W_d at each gridpoint within the waveguide. Evaluating when W_d is non-zero allows for a quick calculation of the local waveguide frequency, i.e. the number of days when

140   each gridpoint lies within a detected waveguide.

4 Climatological waveguide statistics

The waveguide detection algorithm described above is used to identify waveguides in ERA5 data from 1979-2022 during two seasons, winter (December-February in the Northern hemisphere, NH; June - August in the Southern hemisphere, SH) and summer (June-August in the NH; December-February in the SH). First, climatological waveguide statistics maps are presented

145 for both hemispheres. In the subsection following this, composites of days with high vs low waveguide presence in particular regions are presented, to study the circulation associated with 'strong' vs 'weak' waveguide days.

4.1 Waveguide frequency and depth

Climatological waveguide frequencies (fraction of days that each gridpoint lies within a waveguide) are shown for wavenumbers $4 \leq k \leq 7$ during both winter and summer for the NH (Fig. 2) and SH (Fig. 3). It is clear that the waveguides are largely

150 constrained to the sub-tropics and mid-latitudes, as expected based on the location of the climatological jets. The black contours in the figures show the seasonal climatology of the zonally-filtered zonal wind U used as the background flow. Fig. 2 shows a
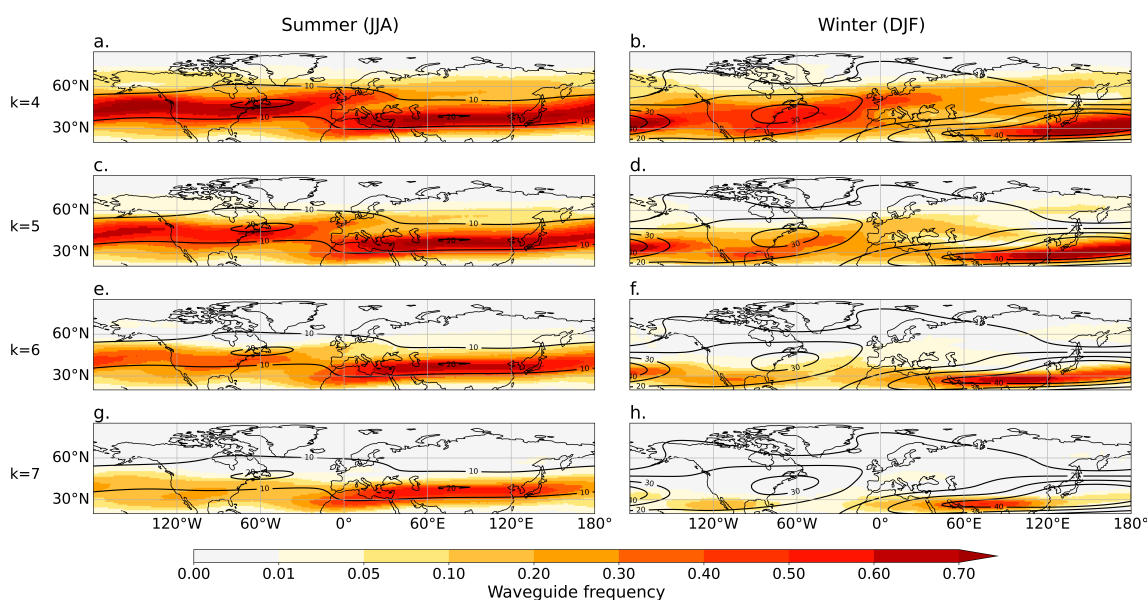
Figure 2. Seasonal waveguide frequency for the NH for summer (left column) and winter (right column) for zonal wavenumbers 4-7. Note the non-linear progression of the color bar at the smallest frequencies.

northward migration of waveguide frequency during summer, in line with the jets, as expected. Despite the strengthening of the NH jet streams during winter, the frequency of waveguides is not substantially greater, and in many regions is, in fact, lower than in summer. Sensitivity studies show this result remains when using a lower-latitude cut-off of 30°N for turning points

155 instead of 20°N.
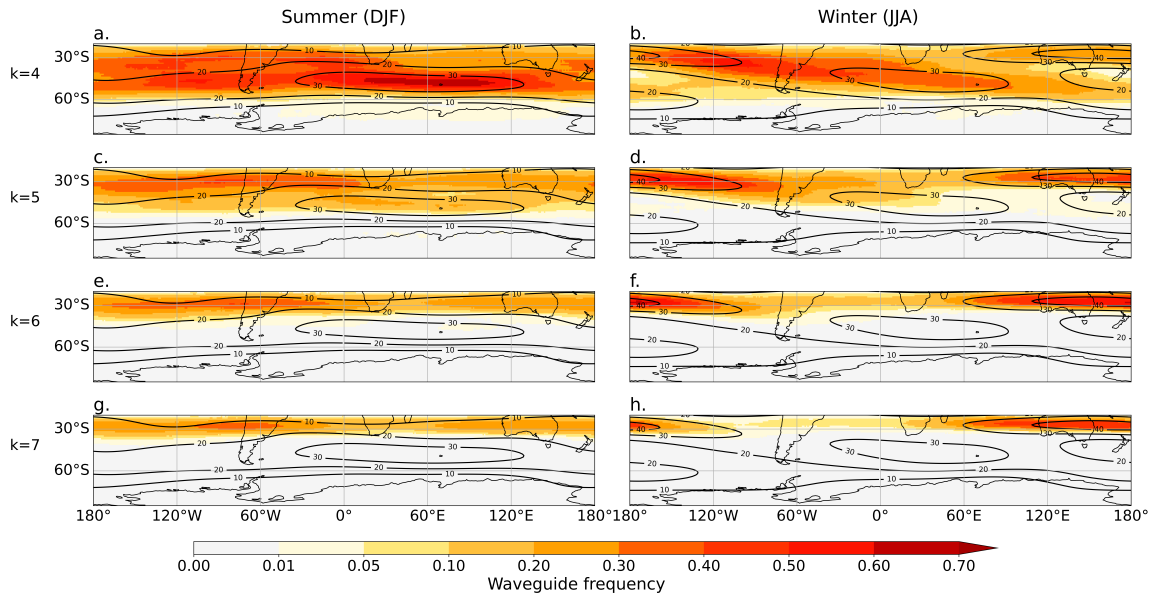
Figure 3. As for Fig. 2, but for the SH. Seasonal waveguide frequency for SH summer (left column) and winter (right column) for zonal wavenumbers 4-7. Note the non-linear progression of the color bar at the smallest frequencies.

In both seasons, the climatological peak waveguide frequency is found slightly equatorward of the climatological jet peak at almost all longitudes (Fig. 2). A similar equatorward shift relative to the jet peak is found in the climatological stationary wavenumber, and can also be seen in the climatological fields calculated by Hoskins and Ambrizzi (1993) and Ambrizzi et al. (1995). Analysis of the terms in Eq. 2 shows that, for the climatological fields, this response is mostly due to the meridional gradient of planetary vorticity term, $\frac{2\Omega cos^2\phi}{a}$, which is larger closer to the equator. It has also been shown that, in some regions, equatorward shifted jets can be stronger (Woollings et al., 2018), and thus might be more likely to act as a waveguide (Manola et al., 2013). This may also contribute to the latitudinal shift between the maximum waveguide frequency and the maximum climatological jet in some regions.

In the SH mid-latitude jet, poleward of 35°S, the algorithm largely only detects waveguides for wavenumbers $k = 4, 5$, and not for higher $k \geq 6$. This is consistent with the values of K_s shown by Ambrizzi et al. (1995) and of the dominant variability in the SH mid-latitudes shown in Manola et al. (2013). The overall waveguide frequency is also typically lower in the SH than in the NH; although this is particularly the case for higher wavenumbers. This is despite faster zonal wind speeds in the SH (c.f. Figs. 2 and 3), which are typically associated with more waveguidability (e.g. Manola et al., 2013). Reduced waveguide frequency with increasing U is however, consistent with the Eq. 1, in which the magnitude of U appears in the denominator of the equation for K_s, and only appears in the second term of β_M(see Eq. 2). Calculations of K_s on linear multiples of the climatological JJA U at various different longitudes confirms that, as U increases in strength but the latitudinal shape remains

constant, K_s decreases in magnitude. If U becomes too weak, then the subtropical turning latitude vanishes, and there is no waveguide; whilst a waveguide exists, however, increasing U reduces the zonal wavenumber within the waveguide.

Average waveguide depths, defined as $K_S - k$ averaged over days only when a waveguide is present, are shown in Figs. 4 (NH) and 5 (SH). Regions where waveguides occur on fewer than 1% of days are masked out to reduce noise. In summer in the NH, the deepest waveguides lie south of the climatological jets, where the meridional gradient of planetary vorticity is high, and U is relatively weak, leading to high values of K_s. The large difference in low-latitude waveguide strength between winter and summer is sensitive to the latitudinal cut-off for a defined waveguide combined with the seasonal cycle in the latitude of the jet. In the mid-latitudes the average waveguide depth is, over most regions, stronger in summer than in winter for low wavenumbers ($k = 4, 5$). These figures also show that, whilst high-latitude waveguides (poleward of 60° N/S) are relatively infrequent (see Fig. 2), when they do occur, they can be relatively strong, with depths greater than 2 or 3 wavenumbers, particularly over the Northern Pacific region.
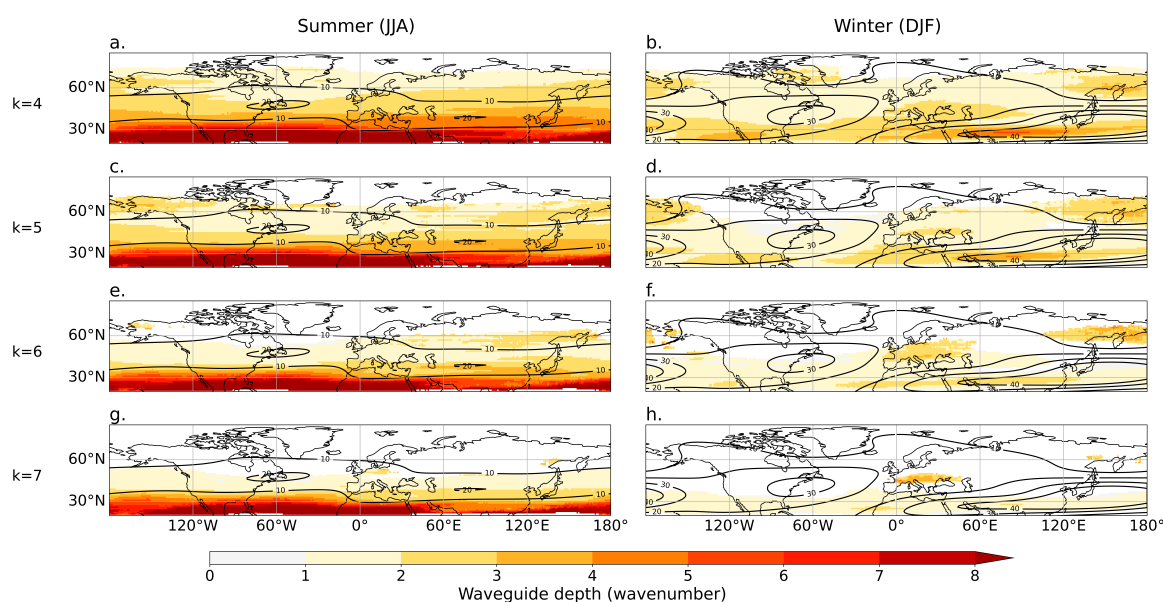
Figure 4. Seasonal waveguide depth ($K_s - k$ when waveguide is present) for the NH for summer (left column) and winter (right column) for zonal wavenumbers 4-7. Fields are masked to where the climatological waveguides frequency shown in Fig. 2 exceeds 0.01, i.e. at least 1% of days have a waveguide present.

4.2 Waveguide composites

To study the conditions associated with strong waveguides, a single 'waveguide strength' metric is defined for each day and each gridpoint by summing the waveguide depths across all wavenumbers for which a waveguide exists. Regional averages of this waveguide strength are made over different regions, and composites are created for both high and low waveguide days –
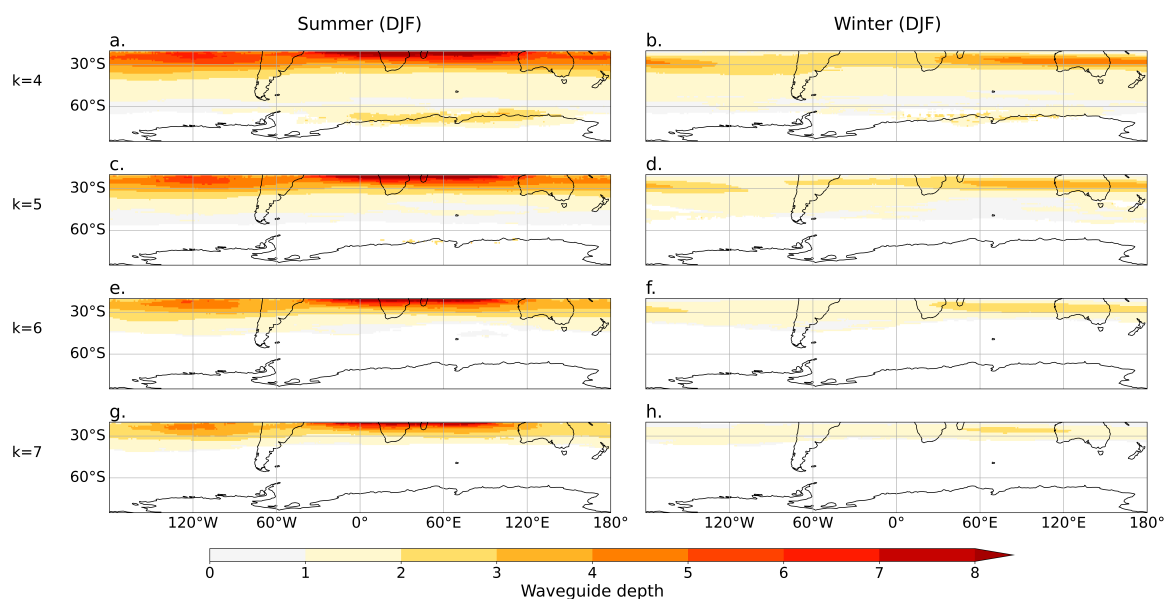
Figure 5. As for Fig. 4, but for the SH. Seasonal waveguide depth ($K_s - k$ when waveguide is present) for SH summer (left column) and winter (right column) for zonal wavenumbers 4-7.

days in which the regional waveguide strength exceeds (is less than) the 90th (10th) percentile. Latitudes are weighted equally, despite waveguides at higher latitudes extending less far zonally due to the curvature of the Earth.

4.2.1 Zonal winds

190   Figure 6 shows the differences in (unfiltered) zonal wind composites between high waveguide days and low waveguide days for four distinct regions in the NH, demonstrating the anomalous background wind conditions associated with particularly strong waveguides in each region. The boxes for the regional averages are shown in the dashed black lines, whilst a single contour of the anomalous waveguide strength (high - low days) is shown in magenta, to demonstrate that different regions are dominated by waveguides at different latitudes, despite each boxed region having the same latitudinal limits (40-60° N); this waveguide

195   field is masked to 0 equatorward of 35° N/S to reduce noise in the plots.

In each region and season analysed in Fig. 6 a 'double jet structure' is present in the vicinity of the waveguide: a region of anomalously low zonal wind at, or immediately to the north of, the region of high waveguide strength, with two regions of anomalously strong zonal winds, one to the north, and one to the south, of the central low anomaly. Such a structure has been previously identified as connected to waveguides (Petoukhov et al., 2013; Kornhuber et al., 2016; Rousi et al., 2022),

200   and is mathematically consistent with the requirement for high $\partial^2 U/\partial\phi^2$ in equation 2. This structure has been described as a strong high-latitude Arctic front jet combined with a strong and narrow subtropical jet (Mann et al., 2018). The meridionally

aligned zonal wind anomalies associated with high waveguide days also shift in latitude with the waveguide region selected (not shown).
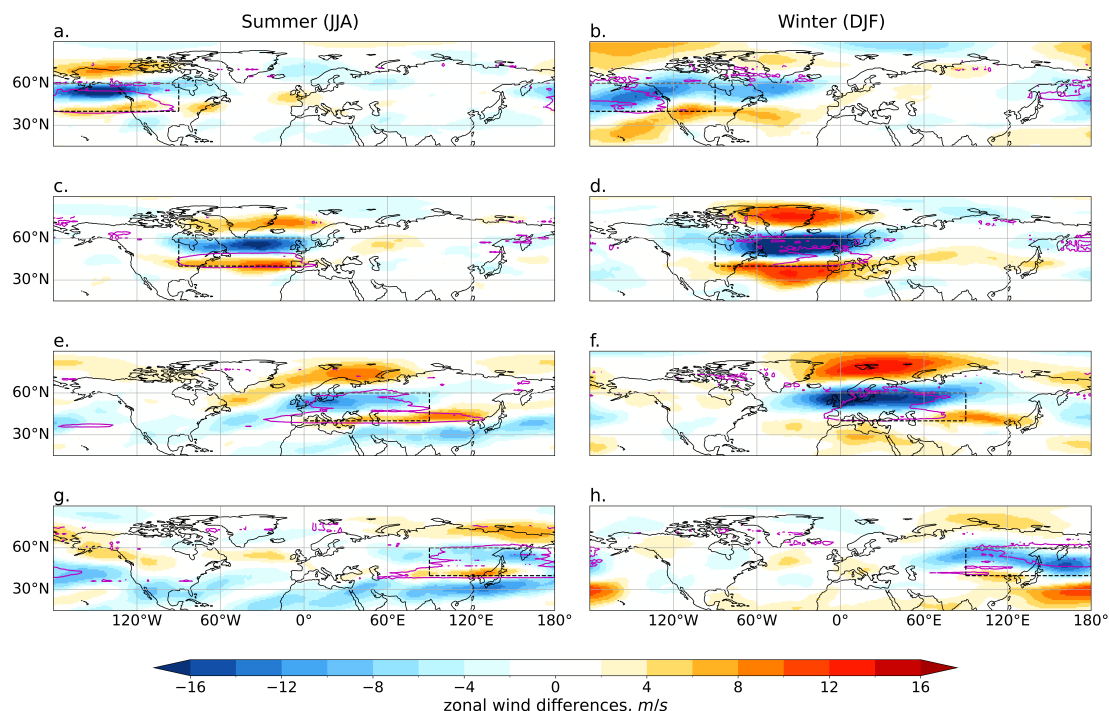
Figure 6. Northern hemisphere $300hPa$ zonal wind ($U300$) differences between composites of the 10% of days with strongest waveguide presence in the black boxed region relative to composites of the 10% of days with the weakest waveguide presence, for different regions (rows) and for summer (JJA; left) and winter (DJF; right).

Similar results can be seen in the SH, shown in Fig. 7, although the anomalous jet structure for waveguides from 0-180°E is typically one high node of anomalously high U, with two nodes of lower U to the north and south, in contrast to the more consistent two anomalous high nodes seen in the NH.

5   Waveguides and atmospheric waves

As an example of further research that can be performed with this waveguide dataset, correlations are calculated between waveguides and quasi-stationary waves to determine whether quasi-stationary waves are indeed correlated with the presence of waveguides, as has been hypothesised (Petoukhov et al., 2016; White et al., 2022). First, smoothed daily climatologies of both waveguides and QSW envelope magnitude were created, by calculating a daily climatology, and then applying an
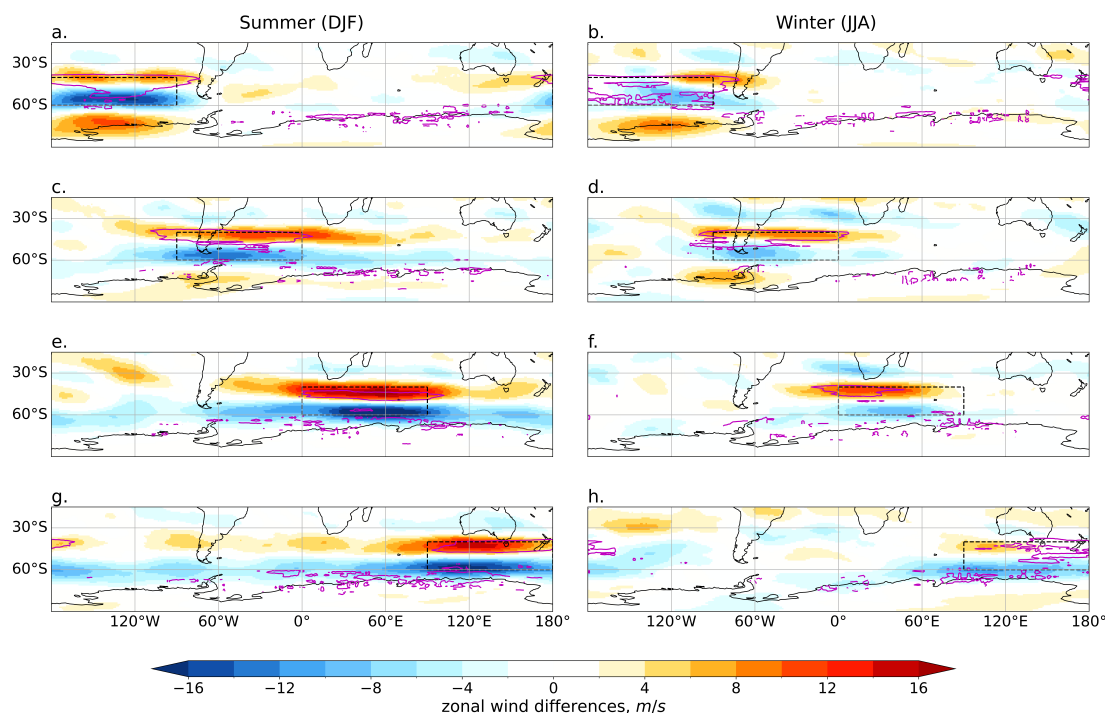
Figure 7. As for Fig. 6, but for the Southern hemisphere. $300hPa$ zonal wind ($U300$) differences between composites of the 10% of days with strongest waveguide presence in the black boxed region relative to composites of the 10% of days with the weakest waveguide presence, for different regions (rows) and for SH summer (left) and winter (right)

order-1 Savitzky-Golay filter with a window length of 61 days. Anomalies from these climatologies were calculated to remove the impacts of any seasonal cycles on observed correlations. As a consequence of the time-filtering of the input data for the calculation of both the waveguides and QSW envelopes, as well as intrinsic atmospheric memory, both fields exhibit auto-

215 correlation. To reduce the impacts of this on the degrees of freedom for calculating the significance of the correlations, both fields are sub-sampled with one sample every 10 days; auto-correlation of the sub-sampled waveguide dataset is under 0.1 almost everywhere.

Pearson correlation coefficients are calculated over time for data in JJA and DJF separately, for QSW envelope values and waveguide strength values (summed over wavenumbers 4-9) averaged over 20° longitude by 5° latitude boxes. Correlation

220 coefficients are shown in Fig. 8, with hatching indicating statistical significance, where p-values have been adjusted to account for the false discovery rate of repeating multiple significance tests over space. The adjustment was performed using scipy.stats.false_discovery_control with the Benjaminini-Yekutieli procedure, as the values are not from independent tests due

to spatial correlation; this is a more conservative test, and thus significance is shown for both $p < 0.1$ (diagonal hatching) and $p < 0.05$ (cross-hatching).
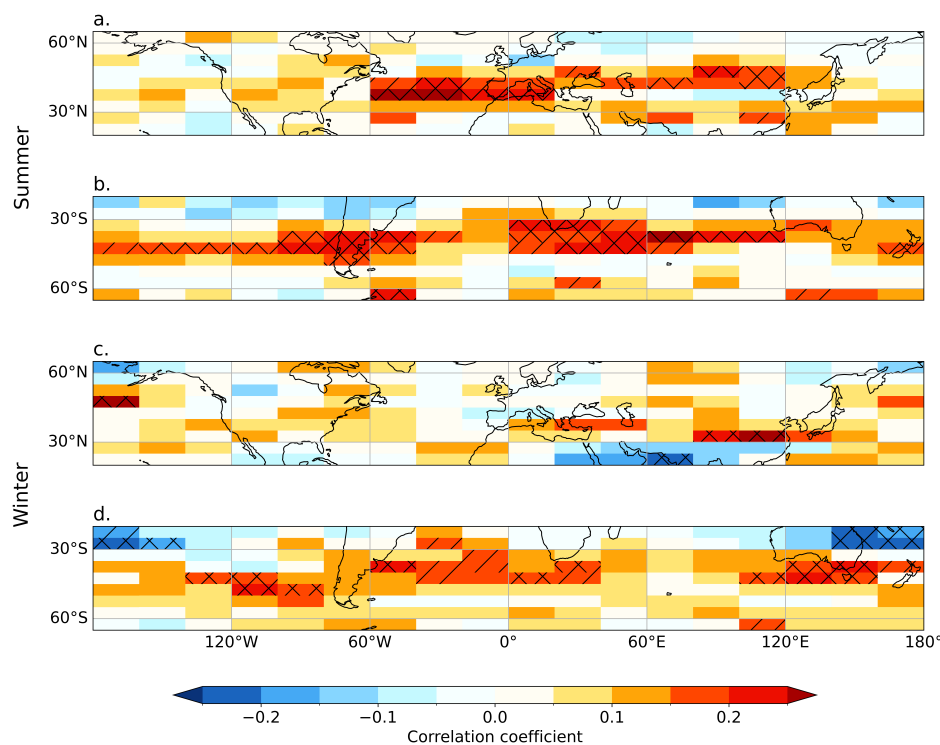
Figure 8. Pearson correlation coefficient between waveguide strength and QSW strength, each averaged over $20°$ longitude $\times$ $5°$ latitude boxes for both summer and winter in both hemispheres. Diagonal hatching indicates regions where the correlation is statistically significant at $p < 0.1$, and cross-hatching at $p < 0.05$.

225 Positive correlations are found between waveguides and quasi-stationary waves over much of the mid-latitudes in summer in both hemispheres. In the northern hemisphere there are relatively strong zonal variations, with significant correlations only over the Atlantic and western Europe, and across China. In the southern hemisphere there is a more zonally symmetric band of positive correlation around $40°$S. The correlations, even where statistically significant, are relatively weak, with typical correlation coefficients of $r < 0.25$.

230 Winter has weaker correlations between waveguides and QSWs than summer (compare Figs. 8c-d with 8a-b), particularly in the NH, where there is limited statistical significance in winter. In the southern hemisphere the zonally symmetric band of positive correlations seen in summer is also present in winter, although with weaker values and less significance.

5.1 Sensitivity tests

As discussed in Section 3, the waveguide identification process includes several parameters, including the wavenumber and
235 time filtering of the background flow, and minimum thresholds for waveguide depth and width. Here we briefly explore the sensitivity of the waveguide climatological frequencies, and the correlations between waveguides and QSWs to these parameters.
As the detection of waveguides presented here depends on meridional gradients, it may be sensitive to the spatial resolution
of the data. This is particularly relevant for applications of a waveguide algorithm to climate model output, which can have
resolutions of $2°$ or lower. To understand the impact of resolution on the detection of waveguides, the $1×1°$ ERA5 data are
240 bilinearly regridded to a $2.5×2.5°$ grid using the Climate Data Operators (CDO) and the waveguide detection procedure is
repeated on these data.

Figure 9 shows the climatological frequency of NH summer waveguides for $k = 6$ for a range of different parameters,
including different wavenumber and time filtering for the pre-processing (panels a-d), different minimum widths and depths
for the waveguide (panels e-f), selecting $30°$N as the equatorward cutoff latitude for turning points (panel g), and using an
245 input dataset at $2.5×2.5°$ resolution (panel h). It is clear from Fig. 9 that differences in climatological waveguide frequency are
relatively small for the range of parameters explored here.

Lastly, I explore the sensitivity of the correlation between waveguides and quasi-stationary waves, again, focussing only on
NH summer. As changes to the climatological frequency are small for the range of parameters explored in Fig. 9, correlations
are calculated for only a subset of the different parameters (Fig. 10a-c), plus the low-latitude cut-off of $30°$N (Fig. 10e) and
250 waveguides calculated on the $2.5×2.5°$ input data (Fig. 10f). The resolution of the QSW data is unchanged, as averages over
boxes larger than the QSW resolution are taken prior to the correlation calculation.

In Fig. 10d I show the correlation when defining the 'waveguide strength', using the maximum waveguide depth across
different wavenumbers in contrast to the sum of waveguide depths used previously. As for the climatological waveguide
frequency, there is relatively little sensitivity to any of these changes explored, and the conclusions remain unchanged.

255 6 Discussion

This paper describes an objective detection algorithm for barotropic atmospheric waveguides on temporally and zonally varying
flow, and some statistics of the waveguides identified by this algorithm, including climatologies and their associations with
quasi-stationary waves. Waveguides are not particularly unusual; in the maxima of the climatological jets, waveguides for
$k \geq 4$ waves occur on over 50% of days in both summer and winter in both hemispheres. Whilst in general waveguides are
260 spatially associated with the jets, as expected, there is broadly an enhanced waveguide frequency in summer over winter, despite
typically weaker jets in summer, highlighting a rather complex relationship between jet strength and barotropic waveguides.
Manola et al. (2013) concluded that 'strong, narrow jets' create good waveguide conditions, and the results shown here may
be indicating the importance of *narrow* over, or at least in addition to, *strong*. Further research is required to fully investigate
this result; however, this suggests that understanding the impacts of anthropogenic climate change on barotropic waveguides is
265 non-trivial, even if we had a clear understanding of how climate change will impact jet strengths.
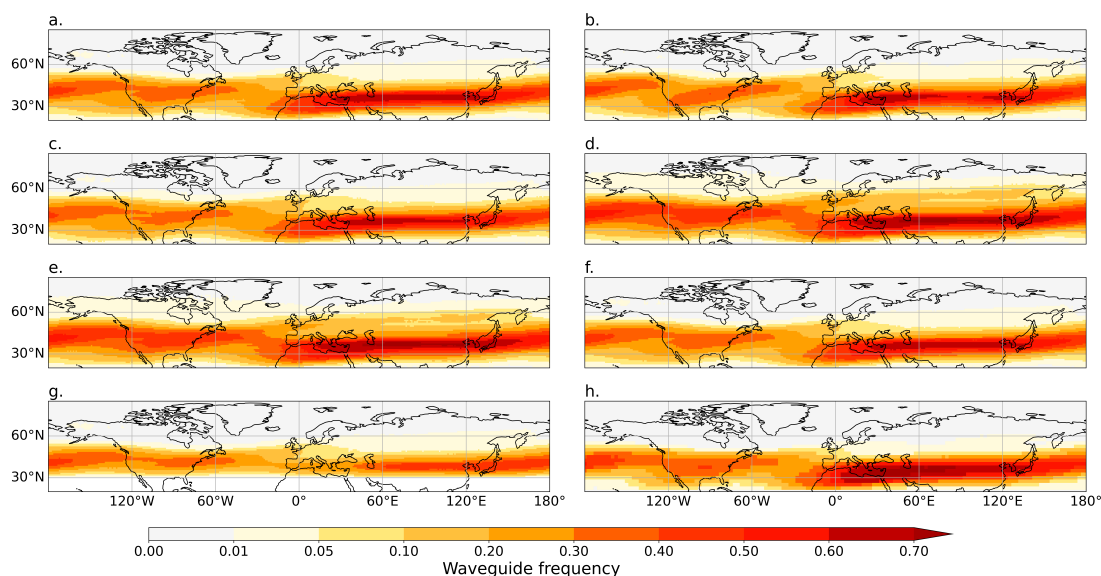
Figure 9. Climatological frequency of NH $k = 6$ waveguides in JJA for different sensitivity parameters and dataset resolution. Panels a-g are all with $1 \times 1°$ resolution data, with panel h with $2.5 \times 2.5°$ data. a. wavelength = 2, time filter = 15, minimum depth = 1, minimum width = 5 (as shown in Fig. 2e); b. wavelength = 3, time filter = 15, minimum depth = 1, minimum width = 5; c. wavelength = 2, time filter = 10, minimum depth = 1, minimum width = 5; d. wavelength = 2, time filter = 15, minimum depth = 1, minimum width = 3; e. wavelength = 2, time filter = 15, minimum depth = 0.1, minimum width = 3; f. wavelength = 2, time filter = 15, minimum depth = 0.5, minimum width = 5; g. as for a. but with the equatorward turning point cut-off at $30°$N; h. as for a. but with $2.5 \times 2.5°$ data.

One of the potential limitations of the turning latitude approach to identifying waveguides used here, in contrast to a PV gradient approach, is that it introduces a binary definition - either a waveguide exists (two turning latitudes exist), or it does not (Wirth, 2020). The algorithm described here attempts to reduce this problem by calculating a waveguide 'depth' for a given zonal wavenumber, k. I then define a total 'waveguide strength' as the sum of the waveguide depths for wavenumbers $4 \geq k \leq 9$. Composites of days with high vs low waveguide strength show clear double jet zonal wind patterns, as previously identified as associated with waveguides (Rousi et al., 2022). This waveguide strength also correlates positively with quasi-stationary wave activity in much of the mid-latitudes. An additional limitation of this method is the missing influence of atmospheric stability, which is captured in a PV waveguide definition (e.g. Xu et al., 2021); work to contrast and compare the turning latitude and PV gradient waveguide definitions would be very interesting.

Figures 8 and 10 show significant positive correlations between the presence of strong waveguides and the presence of strong quasi-stationary waves across the mid-latitude, although correlations are relatively weak, and are not significant in all regions in both seasons. Positive correlations are typically stronger in the southern hemisphere, with significant correlations in the northern hemisphere limited to the Atlantic and Eurasian regions in summer. This connection has been hypothesised,
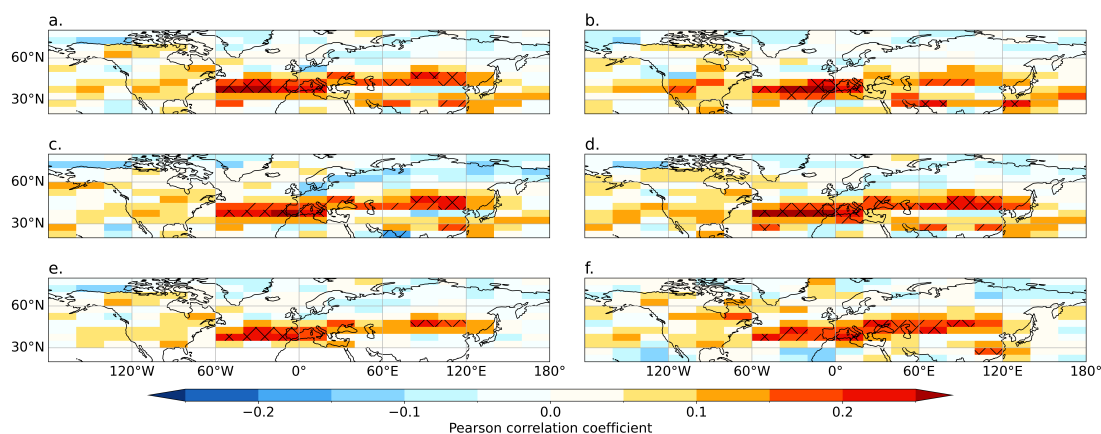
Figure 10. Correlation coefficient between waveguide strength and QSW amplitude, each averaged over $20°$ longitude $\times$ $5°$ latitude boxes, for NH summer for different sensitivity parameters, dataset resolution, and waveguide strength definition. Unless otherwise stated, the resolution is $1\times1°$ resolution and waveguide strength is the sum of waveguide depth over wavenumbers 4-9. a. wavelength = 2, time filter = 15, minimum depth = 1, minimum width = 5 (identical to Fig. 8a); b. as for a. but with time filter = 10 for both waveguides and QSWs; c. as for a. but with minimum depth = 0.1, minimum width = 3; d. as for a. but with waveguide strength as the maximum waveguide depth over wavenumbers 4-9; e. as for a. but with the waveguide turning point cut-off at $30°$N instead of $20°$N; f. as for a. but with $2.5\times2.5°$ data.

and shown to some extent in monthly data in previous studies (Petoukhov et al., 2013, 2016; Mann et al., 2017). Notably, the strongest correlation between waveguides and QSWs in the NH is found in summer over western Europe (and upstream over the Atlantic), a region which has seen a noticeable increase in summer heat extremes in recent years associated with changing atmospheric circulation patterns (Vautard et al., 2023). These changing atmospheric circulation patterns may be connected to trends in Rossby waves (Kornhuber et al., 2019), and possibly Rossby waveguides. It has been hypothesised that Arctic amplification may be reducing the speed of the jet, potentially changing waveguide frequency or strength, and subsequently changes in amplified Rossby waves (e.g. Coumou et al., 2014; Mann et al., 2018; Coumou et al., 2018), although there is not yet consensus on this theory (Screen and Simmonds, 2013a, b; Blackport and Screen, 2020), and aerosols may also have played an equal or stronger role in recent trends in some regions (Dong et al., 2022). The strong connection between waveguides and quasi-stationary waves over Europe warrants further investigation as to the role changing waveguides may have had on recent trends in heatwaves.

It should be noted that causality from waveguides to QSWs has not been established here. Atmospheric blocks, which would show up as a positive anomaly in the quasi-stationary wave metric, can lead to a double jet structure that increases waveguide probability (Wirth and Polster, 2021). Using a zonalized flow (Methven and Berrisford, 2015), as performed by (Polster and Wirth, 2023) may provide an improved separation of the waves and the background flow; repeating this waveguide detection and analysis on background U derived using a zonalization technique would be very interesting. Because of this connection between waves and waveguides, caution is required in interpreting the direction of any causality between waveguides, quasi-

stationary waves and heatwaves. The waveguide dataset produced in this study could be an important step in establishing any causality, and its direction.

7 Conclusions

Zonally-varying barotropic waveguides are identified in ERA5 data from 1980-2022 on daily temporal resolution. Climatolog-
300 ical waveguide statisics show that near the centre of the mid-latitude jets a waveguide exists on up to 70% of days. Waveguides are found to be slightly more frequent in summer than winter, and more frequent in the Northern hemisphere than the Southern. A double jet structure is found to be associated with strong waveguide days, particularly over the North Atlantic and European regions. Positive correlations are found between waveguide strength and the presence of strong quasi-stationary waves, par-
ticularly in the Southern Hemisphere. In the Northern hemisphere, statistically significant correlations are found only during
305 summer over the North Atlantic, Europe and Asia.

Data availability. ERA5 data were downloaded from the Copernicus Data Store (CDS): https://cds.climate.copernicus.eu/cdsapp!/dataset/reanalysis-era5-pressure-levels

Appendix A: Mercator Projection

$$x = a\lambda \tag{A1}$$

310

$$y = a \ln\left[\frac{1+\sin\phi}{\cos\phi}\right] \tag{A2}$$

$$\frac{\partial y}{\partial \phi} = a\frac{\cos\phi}{1+\sin\phi}\frac{\partial}{\partial \phi}\left(\frac{1+\sin\phi}{\cos\phi}\right) = a\frac{\cos\phi}{1+\sin\phi}\left(\frac{1+\sin\phi}{\cos^2\phi}\right) = \frac{a}{\cos\phi} \tag{A3}$$

315 $$\frac{\partial}{\partial y} = \frac{\cos\phi}{a}\frac{\partial}{\partial \phi} \tag{A4}$$

Author contributions. The author completed all aspects of this work.

Competing interests. The author declares no competing interests

References

320   Ali, S. M., Martius, O., and Röthlisberger, M.: Recurrent Rossby Wave Packets Modulate the Persistence of Dry and Wet Spells Across the Globe, Geophysical Research Letters, 48, e2020GL091 452, https://doi.org/10.1029/2020GL091452, 2021.

Ambrizzi, T., Hoskins, B. J., and Hsu, H.-H.: Rossby Wave Propagation and Teleconnection Patterns in the Austral Winter, Journal of the Atmospheric Sciences, 52, 3661–3672, https://doi.org/10.1175/1520-0469(1995)052<3661:RWPATP>2.0.CO;2, 1995.

Andrews, D. G.: Wave–Mean-Flow Interaction in the Middle Atmosphere, in: Advances in Geophysics, edited by Saltzman, B., vol. 28 of
325   *Issues in Atmospheric and Oceanic Modeling*, pp. 249–275, Elsevier, https://doi.org/10.1016/S0065-2687(08)60226-5, 1985.

Blackburn, M., Methven, J., and Roberts, N.: Large-scale context for the UK floods in summer 2007, Weather, 63, 280–288, https://doi.org/10.1002/wea.322, 2008.

Blackport, R. and Screen, J. A.: Insignificant effect of Arctic amplification on the amplitude of midlatitude atmospheric waves, Science Advances, 6, eaay2880, https://doi.org/10.1126/sciadv.aay2880, publisher: American Association for the Advancement of Science, 2020.

330   Bosart, L. F., Hakim, G. J., Tyle, K. R., Bedrick, M. A., Bracken, W. E., Dickinson, M. J., and Schultz, D. M.: Large-Scale Antecedent Conditions Associated with the 12–14 March 1993 Cyclone ("Superstorm '93") over Eastern North America, Monthly Weather Review, 124, 1865–1891, https://doi.org/10.1175/1520-0493(1996)124<1865:LSACAW>2.0.CO;2, 1996.

Branstator, G.: Horizontal Energy propagation in a Barotropic Atmosphere with Meridional and Zonal Structure, Journal of the Atmospheric Sciences, 40, 1689–1708, https://doi.org/10.1175/1520-0469(1983)040<1689:HEPIAB>2.0.CO;2, 1983.

335   Branstator, G.: Long-Lived Response of the Midlatitude Circulation and Storm Tracks to Pulses of Tropical Heating, Journal of Climate, 27, 8809–8826, https://doi.org/10.1175/JCLI-D-14-00312.1, 2014.

Branstator, G. and Teng, H.: Tropospheric Waveguide Teleconnections and Their Seasonality, Journal of the Atmospheric Sciences, 74, 1513–1532, https://doi.org/10.1175/JAS-D-16-0305.1, 2017.

Chen, G., Lu, J., Burrows, D. A., and Leung, L. R.: Local finite-amplitude wave activity as an objective diagnostic of midlatitude extreme
340   weather, Geophysical Research Letters, 42, https://doi.org/10.1002/2015GL066959, 2015.

Coumou, D., Petoukhov, V., Rahmstorf, S., Petri, S., and Schellnhuber, H. J.: Quasi-resonant circulation regimes and hemispheric synchronization of extreme weather in boreal summer, Proceedings of the National Academy of Sciences, 111, 12 331–12 336, https://doi.org/10.1073/pnas.1412797111, publisher: Proceedings of the National Academy of Sciences, 2014.

Coumou, D., Di Capua, G., Vavrus, S., Wang, L., and Wang, S.: The influence of Arctic amplification on mid-latitude summer circulation,
345   Nature Communications, 9, 2959, https://doi.org/10.1038/s41467-018-05256-8, publisher: Nature Publishing Group, 2018.

Ding, Q. and Wang, B.: Circumglobal Teleconnection in the Northern Hemisphere Summer, Journal of Climate, 18, 3483–3505, https://doi.org/10.1175/JCLI3473.1, 2005.

Dong, B., Sutton, R. T., Shaffrey, L., and Harvey, B.: Recent decadal weakening of the summer Eurasian westerly jet attributable to anthropogenic aerosol emissions, Nature Communications, 13, 1148, https://doi.org/10.1038/s41467-022-28816-5, publisher: Nature Publishing
350   Group, 2022.

Francis, J. A. and Vavrus, S. J.: Evidence linking Arctic amplification to extreme weather in mid-latitudes, Geophysical Research Letters, 39, https://doi.org/10.1029/2012GL051000, _eprint: https://onlinelibrary.wiley.com/doi/pdf/10.1029/2012GL051000, 2012.

Giannakaki, P. and Martius, O.: An Object-Based Forecast Verification Tool for Synoptic-Scale Rossby Waveguides, Weather and Forecasting, 31, 937–946, https://doi.org/10.1175/WAF-D-15-0147.1, 2016.

355 Held, I. M., Panetta, R. L., and Pierrehumbert, R. T.: Stationary External Rossby Waves in Vertical Shear, Journal of the Atmospheric
Sciences, 42, 865–883, https://doi.org/10.1175/1520-0469(1985)042<0865:SERWIV>2.0.CO;2, publisher: American Meteorological So-
ciety Section: Journal of the Atmospheric Sciences, 1985.

Held, I. M., Ting, M., and Wang, H.: Northern Winter Stationary Waves: Theory and Modeling, Journal of Climate, 15, 2125–2144,
https://doi.org/10.1175/1520-0442(2002)015<2125:NWSWTA>2.0.CO;2, 2002.

360 Hersbach, H., Bell, B., Berrisford, P., Hirahara, S., Horányi, A., Muñoz-Sabater, J., Nicolas, J., Peubey, C., Radu, R., Schepers, D., Simmons,
A., Soci, C., Abdalla, S., Abellan, X., Balsamo, G., Bechtold, P., Biavati, G., Bidlot, J., Bonavita, M., De Chiara, G., Dahlgren, P., Dee,
D., Diamantakis, M., Dragani, R., Flemming, J., Forbes, R., Fuentes, M., Geer, A., Haimberger, L., Healy, S., Hogan, R. J., Hólm, E.,
Janisková, M., Keeley, S., Laloyaux, P., Lopez, P., Lupu, C., Radnoti, G., De Rosnay, P., Rozum, I., Vamborg, F., Villaume, S., and Thépaut,
J.: The ERA5 global reanalysis, Quarterly Journal of the Royal Meteorological Society, 146, 1999–2049, https://doi.org/10.1002/qj.3803,
365 2020.

Hersbach, H., Bell, B., Berrisford, P., Biavati, G., Horányi, A., Muñoz Sabater, J., Nicolas, J., Peubey, C., Radu, R., Rozum, I.,
Schepers, D., Simmons, A., Soci, C., Dee, D., and Thépaut, J.-N.: ERA5 hourly data on pressure levels from 1940 to present,
https://doi.org/10.24381/cds.bd0915c6, 2023.

Hirata, F. E. and Grimm, A. M.: The role of synoptic and intraseasonal anomalies in the life cycle of summer rainfall extremes over South
370 America, Climate Dynamics, 46, 3041–3055, https://doi.org/10.1007/s00382-015-2751-6, 2016.

Hoskins, B. and Woollings, T.: Persistent Extratropical Regimes and Climate Extremes, Current Climate Change Reports, 1, 115–124,
https://doi.org/10.1007/s40641-015-0020-8, 2015.

Hoskins, B. J. and Ambrizzi, T.: Rossby Wave Propagation on a Realistic Longitudinally Varying Flow, Journal of the Atmospheric Sciences,
50, 1661–1671, https://doi.org/10.1175/1520-0469(1993)050<1661:RWPOAR>2.0.CO;2, 1993.

375 Hoskins, B. J. and Karoly, D. J.: The Steady Linear Response of a Spherical Atmosphere to Thermal and Orographic Forcing, Journal of the
Atmospheric Sciences, 38, 1179–1196, https://doi.org/10.1175/1520-0469(1981)038<1179:TSLROA>2.0.CO;2, 1981.

Hsu, H.-H. and Lin, S.-H.: Global Teleconnections in the 250-mb Streamfunction Field during the Northern Hemisphere Winter, Monthly
Weather Review, 120, 1169–1190, https://doi.org/10.1175/1520-0493(1992)120<1169:GTITMS>2.0.CO;2, 1992.

Jiménez-Esteve, B., Kornhuber, K., and Domeisen, D. I. V.: Heat Extremes Driven by Amplification of Phase-Locked Circum-
380 global Waves Forced by Topography in an Idealized Atmospheric Model, Geophysical Research Letters, 49, e2021GL096 337,
https://doi.org/10.1029/2021GL096337, 2022.

Kornhuber, K., Petoukhov, V., Petri, S., Rahmstorf, S., and Coumou, D.: Evidence for wave resonance as a key mechanism for generating
high-amplitude quasi-stationary waves in boreal summer, Climate Dynamics, pp. 1–19, https://doi.org/10.1007/s00382-016-3399-6, 2016.

Kornhuber, K., Osprey, S., Coumou, D., Petri, S., Petoukhov, V., Rahmstorf, S., and Gray, L.: Extreme weather events in early summer
385 2018 connected by a recurrent hemispheric wave-7 pattern, Environmental Research Letters, 14, 054 002, https://doi.org/10.1088/1748-
9326/ab13bf, 2019.

Limpasuvan, V. and Hartmann, D. L.: Wave-Maintained Annular Modes of Climate Variability, Journal of Climate, 13, 4414–4429,
https://doi.org/10.1175/1520-0442(2000)013<4414:WMAMOC>2.0.CO;2, publisher: American Meteorological Society Section: Journal
of Climate, 2000.

390 Lorenz, D. J. and Hartmann, D. L.: Eddy–Zonal Flow Feedback in the Northern Hemisphere Winter, Journal of Climate, 16, 1212–1227,
https://doi.org/10.1175/1520-0442(2003)16<1212:EFFITN>2.0.CO;2, publisher: American Meteorological Society Section: Journal of
Climate, 2003.

Mann, M. E., Rahmstorf, S., Kornhuber, K., Steinman, B. A., Miller, S. K., and Coumou, D.: Influence of Anthropogenic Climate Change on Planetary Wave Resonance and Extreme Weather Events, Scientific Reports, 7, 45 242, https://doi.org/10.1038/srep45242, 2017.

395 Mann, M. E., Rahmstorf, S., Kornhuber, K., Steinman, B. A., Miller, S. K., Petri, S., and Coumou, D.: Projected changes in persistent extreme summer weather events: The role of quasi-resonant amplification, Science Advances, 4, eaat3272, https://doi.org/10.1126/sciadv.aat3272, publisher: American Association for the Advancement of Science, 2018.

Manola, I., Selten, F., de Vries, H., and Hazeleger, W.: "Waveguidability" of idealized jets, Journal of Geophysical Research: Atmospheres, 118, 10,432–10,440, https://doi.org/10.1002/jgrd.50758, 2013.

400 Marengo, J. A., Ambrizzi, T., Kiladis, G., and Liebmann, B.: Upper-air wave trains over the Pacific Ocean and wintertime cold surges in tropical-subtropical South America leading to Freezes in Southern and Southeastern Brazil, Theoretical and Applied Climatology, 73, 223–242, https://doi.org/10.1007/s00704-001-0669-x, 2002.

Martius, O., Schwierz, C., and Davies, H. C.: Tropopause-Level Waveguides, Journal of the Atmospheric Sciences, 67, 866–879, https://doi.org/10.1175/2009JAS2995.1, 2010.

405 McKinnon, K. A., Rhines, A., Tingley, M. P., and Huybers, P.: Long-lead predictions of eastern United States hot days from Pacific sea surface temperatures, Nature Geoscience, 9, 389–394, https://doi.org/10.1038/ngeo2687, 2016.

Methven, J. and Berrisford, P.: The slowly evolving background state of the atmosphere, Quarterly Journal of the Royal Meteorological Society, 141, 2237–2258, https://doi.org/10.1002/qj.2518, _eprint: https://onlinelibrary.wiley.com/doi/pdf/10.1002/qj.2518, 2015.

Nakamura, N. and Solomon, A.: Finite-Amplitude Wave Activity and Mean Flow Adjustments in the Atmospheric General Circulation. Part
410 II: Analysis in the Isentropic Coordinate, Journal of the Atmospheric Sciences, 68, 2783–2799, https://doi.org/10.1175/2011JAS3685.1, publisher: American Meteorological Society Section: Journal of the Atmospheric Sciences, 2011.

Nakamura, N. and Zhu, D.: Finite-Amplitude Wave Activity and Diffusive Flux of Potential Vorticity in Eddy–Mean Flow Interaction, Journal of the Atmospheric Sciences, 67, 2701–2716, https://doi.org/10.1175/2010JAS3432.1, 2010.

Parker, T. J., Berry, G. J., and Reeder, M. J.: The Structure and Evolution of Heat Waves in Southeastern Australia, Journal of Climate, 27,
415 5768–5785, https://doi.org/10.1175/JCLI-D-13-00740.1, 2014.

Petoukhov, V., Rahmstorf, S., Petri, S., and Schellnhuber, H. J.: Quasiresonant amplification of planetary waves and recent Northern Hemisphere weather extremes, Proceedings of the National Academy of Sciences, 110, 5336–5341, https://doi.org/10.1073/pnas.1222000110, 2013.

Petoukhov, V., Petri, S., Rahmstorf, S., Coumou, D., Kornhuber, K., and Schellnhuber, H. J.: Role of quasiresonant planetary wave
420 dynamics in recent boreal spring-to-autumn extreme events, Proceedings of the National Academy of Sciences, 113, 6862–6867, https://doi.org/10.1073/pnas.1606300113, 2016.

Polster, C. and Wirth, V.: A New Atmospheric Background State to Diagnose Local Waveguidability, Geophysical Research Letters, 50, e2023GL106 166, https://doi.org/10.1029/2023GL106166, _eprint: https://onlinelibrary.wiley.com/doi/pdf/10.1029/2023GL106166, 2023.

425 Rossby, C.-G.: Relation between Variations in the Intensity of the Zonal Circulation of the Atmosphere and the Displacements of the Semi-Permanent Centers of Action, Journal of Marine Research, 2, 38–55, 1939.

Rousi, E., Kornhuber, K., Beobide-Arsuaga, G., Luo, F., and Coumou, D.: Accelerated western European heatwave trends linked to more-persistent double jets over Eurasia, Nature Communications, 13, 3851, https://doi.org/10.1038/s41467-022-31432-y, 2022.

Röthlisberger, M., Frossard, L., Bosart, L. F., Keyser, D., and Martius, O.: Recurrent Synoptic-Scale Rossby Wave Patterns and Their Effect
430 on the Persistence of Cold and Hot Spells, Journal of Climate, 32, 3207–3226, https://doi.org/10.1175/JCLI-D-18-0664.1, 2019.

Schubert, S., Wang, H., and Suarez, M.: Warm Season Subseasonal Variability and Climate Extremes in the Northern Hemisphere: The Role of Stationary Rossby Waves, Journal of Climate, 24, 4773–4792, https://doi.org/10.1175/JCLI-D-10-05035.1, 2011.

Screen, J. A. and Simmonds, I.: Caution needed when linking weather extremes to amplified planetary waves, Proceedings of the National Academy of Sciences, 110, E2327–E2327, https://doi.org/10.1073/pnas.1304867110, publisher: Proceedings of the National Academy of Sciences, 2013a.

Screen, J. A. and Simmonds, I.: Exploring links between Arctic amplification and mid-latitude weather, Geophysical Research Letters, 40, 959–964, https://doi.org/10.1002/grl.50174, _eprint: https://onlinelibrary.wiley.com/doi/pdf/10.1002/grl.50174, 2013b.

Screen, J. A. and Simmonds, I.: Amplified mid-latitude planetary waves favour particular regional weather extremes, Nature Climate Change, 4, 704–709, https://doi.org/10.1038/nclimate2271, 2014.

Teng, H., Branstator, G., Wang, H., Meehl, G. A., and Washington, W. M.: Probability of US heat waves affected by a subseasonal planetary wave pattern, Nature Geoscience, 6, 1056–1061, https://doi.org/10.1038/ngeo1988, 2013.

Vautard, R., Cattiaux, J., Happé, T., Singh, J., Bonnet, R., Cassou, C., Coumou, D., D'Andrea, F., Faranda, D., Fischer, E., Ribes, A., Sippel, S., and Yiou, P.: Heat extremes in Western Europe increasing faster than simulated due to atmospheric circulation trends, Nature Communications, 14, 6803, https://doi.org/10.1038/s41467-023-42143-3, publisher: Nature Publishing Group, 2023.

Vries, D. and Jan, A.: A global climatological perspective on the importance of Rossby wave breaking and intense moisture transport for extreme precipitation events, Weather and Climate Dynamics, 2, 129–161, https://doi.org/10.5194/wcd-2-129-2021, 2021.

White, R. H., Battisti, D. S., and Roe, G. H.: Mongolian Mountains Matter Most: Impacts of the Latitude and Height of Asian Orography on Pacific Wintertime Atmospheric Circulation, Journal of Climate, 30, 4065–4082, https://doi.org/10.1175/JCLI-D-16-0401.1, 2017.

White, R. H., Kornhuber, K., Martius, O., and Wirth, V.: From Atmospheric Waves to Heatwaves: A Waveguide Perspective for Understanding and Predicting Concurrent, Persistent, and Extreme Extratropical Weather, Bulletin of the American Meteorological Society, 103, E923–E935, https://doi.org/10.1175/BAMS-D-21-0170.1, publisher: American Meteorological Society Section: Bulletin of the American Meteorological Society, 2022.

Wirth, V.: Waveguidability of idealized midlatitude jets and the limitations of ray tracing theory, Weather and Climate Dynamics, 1, 111–125, https://doi.org/10.5194/wcd-1-111-2020, publisher: Copernicus GmbH, 2020.

Wirth, V. and Polster, C.: The Problem of Diagnosing Jet Waveguidability in the Presence of Large-Amplitude Eddies, Journal of the Atmospheric Sciences, 78, 3137–3151, https://doi.org/10.1175/JAS-D-20-0292.1, 2021.

Wirth, V., Riemer, M., Chang, E. K. M., and Martius, O.: Rossby Wave Packets on the Midlatitude Waveguide—A Review, Monthly Weather Review, 146, 1965–2001, https://doi.org/10.1175/MWR-D-16-0483.1, 2018.

Wolf, G. and Wirth, V.: Implications of the Semigeostrophic Nature of Rossby Waves for Rossby Wave Packet Detection, Monthly Weather Review, 143, 26–38, https://doi.org/10.1175/MWR-D-14-00120.1, 2015.

Wolf, G., Brayshaw, D. J., Klingaman, N. P., and Czaja, A.: Quasi-stationary waves and their impact on European weather and extreme events, Quarterly Journal of the Royal Meteorological Society, 144, 2431–2448, https://doi.org/10.1002/qj.3310, 2018.

Woollings, T., Barnes, E., Hoskins, B., Kwon, Y.-O., Lee, R. W., Li, C., Madonna, E., McGraw, M., Parker, T., Rodrigues, R., Spensberger, C., and Williams, K.: Daily to Decadal Modulation of Jet Variability, Journal of Climate, 31, 1297–1314, https://doi.org/10.1175/JCLI-D-17-0286.1, publisher: American Meteorological Society Section: Journal of Climate, 2018.

Xu, P., Wang, L., Vallis, G. K., Geen, R., Screen, J. A., Wu, P., Ding, S., Huang, P., and Chen, W.: Amplified Waveguide Teleconnections Along the Polar Front Jet Favor Summer Temperature Extremes Over Northern Eurasia, Geophysical Research Letters,

48, e2021GL093 735, https://doi.org/10.1029/2021GL093735, _eprint: https://onlinelibrary.wiley.com/doi/pdf/10.1029/2021GL093735, 2021.

470   Zimin, A. V., Szunyogh, I., Patil, D. J., Hunt, B. R., and Ott, E.: Extracting Envelopes of Rossby Wave Packets, Monthly Weather Review, 131, 1011–1017, https://doi.org/10.1175/1520-0493(2003)131<1011:EEORWP>2.0.CO;2, 2003.